Journal of Superconductivity and Novel Magnetism (2021) 34:1215–1223
https://doi.org/10.1007/s10948-021-05803-3

ORIGINAL PAPER

Thermoelectric Potential of $OsAl_2$ Chimney Ladder Compound: a Theoretical Investigation

Rezki Mesbout[1] · Ali Bentouaf[2,3] · Brahim Aïssa[4,5]

Received: 18 October 2020 / Accepted: 4 January 2021 / Published online: 12 February 2021

Abstract
We report on the theoretical study of the structural and electronic properties of $OsAl_2$ compound belonging to chimney ladder (CLs) phases. We used the full potential linearized augmented plane wave (FP-LAPW) method based on the density functional theory (DFT). The Boltzmann semi-classical transport equations were employed to investigate the thermoelectric properties. The type-$MoSi_2$ structure was found to be the most favorable phase to crystallize $OsAl_2$. In addition, the gap between the valence and conduction bands was calculated to be about 0.358 eV, indicating thereby an indirect band gap semiconducting nature. The thermoelectric properties, such as Seebeck coefficient, electrical conductivity, power factor, thermal conductivity, and figure of merit, were also calculated as a function of chemical potential, for a large range of temperatures, starting from room temperature and ending at 900°K. Our results demonstrate high thermoelectric performance with an important merit factor value of about 0.90, which is close to unity, hence revealing that the investigated $OsAl_2$ material has a true potential for thermoelectric applications.

Keywords CLs phases · Thermoelectric materials · FP-LAPW · Electronic properties · Seebeck coefficient · Band structure

1 Introduction

Intermetallic is the short designation for intermetallic phases and compounds that result from the combination of different metals which form a diverse class of materials [1]. Some intermetallic compounds are interesting functional materials; others have gained attention as structural materials for high temperature applications. In comparison with metallic materials, intermetallic compounds exhibit interesting mechanical and thermal properties such as high mechanical resistance to high temperature, low density, high melting point temperature, good corrosion resistance and thermal stability [2–4] which are often superior to ordinary metals. Most of the intermetallic material market targets the automotive and aeronautic sectors, as well as gas turbines where these compounds are considered to be structural materials used in the form of coatings in order to improve the properties of rigidity, lightness, and ductility. Another new field of application of intermetallic compounds is the storage of hydrogen.

Since the discovery of thermoelectric effects by Seebeck, Peltier, and Thomson in the nineteenth century [5–7], the thermoelectricity has never ceased to feed an increasing interest both from a fundamental and industrial point of view. Thermoelectricity allows to generate an electric current from a temperature gradient (Seebeck effect) and conversely to generate a temperature difference from an electric current (Peltier effect) [6]. During the last two decades, two main topics have been deeply explored, namely, (i) the optimization of existing thermoelectric materials and (ii) the search for new compounds guided by specific criteria on the band structure and/or on the complexity of the crystal lattice [7]. This effort has led to the discovery of new families of very promising

✉ Ali Bentouaf
lilo.btf@gmail.com; ali.bentouaf@univ-saida.dz

[1] Faculty of Exact Sciences, University of Djilali Liabes, 22000 Sidi Bel Abbes, Algeria

[2] Faculty of Technology, University of Dr. Moulay Tahar, 20000 Saida, Algeria

[3] Laboratory of Physical Chemistry of Advanced Materials, University of Djillali Liabes, BP 89, 22000 Sidi Bel Abbes, Algeria

[4] Space & Photonics Division, MPB Communications Inc., 151 Hymus Boulevard, Pointe Claire, Quebec, Canada

[5] Qatar Environment and Energy Research Institute (QEERI), Hamad Bin Khalifa University, Qatar-Foundation, P.O. Box 5825, Doha, Qatar

thermoelectric materials for electricity generation [8]. The thermoelectric effect and optical characteristics of intermetallic compounds offer a paramount platform as multifunctional materials for advanced electronic devices. The chimney ladder phases are one of the most known intermetallic compounds and are characterized by the composition of T_nX_m (Tis a transition metal element belonging to the 4–9 columns of the periodic table of elements and X represents the elements of 13 to 15 ones). The unit cells of these structures all contain *n* pseudo-cells of a β-Sn like arrangement of T metal atoms stacked along the [001] direction, and m pseudo-cells of the X component stretched out to fill up the cell, hence the name chimney ladder phases. In general, NCLs compounds become intrinsic semiconductors when obey to the 14-electronrule (the Fermi level located in the middle of a narrow band gap and the valence electron count (VEC) per number of T atoms equal to fourteen (14) [9–12]. The gap formation in TX_2compounds is mainly due to the hybridization of T-3d with X-s, p states. Therefore $RuAl_2$, $RuGa_2$, and $OsAl_2$ have completely filled bands and are expected to show semiconducting properties.

These compounds have been proposed as thermoelectric energy materials due to their low lattice heat conductivity and to their semiconducting nature [13–19].Researches were focused so far to reduce the heat conduction without reducing the electronic flow since low thermal conductivity is favorable for achieving high thermoelectric figure of merit. The family of TE materials includes, among others, high manganese silicides (HMS) (Mn_4Si_7 [20], $Mn_{11}Si_{19}$ [21], and $Mn_{15}Si_{26}$ [22]), which are known to exhibit a high Seebeck coefficient and low thermal conductivity, simultaneously [16, 23–25]. The thermoelectric performance is evaluated with the dimensionless figure of merit $ZT = S^2\sigma$ T/K, where *S*, σ, k, and T are the Seebeck coefficient, electrical conductivity, thermal conductivity, and absolute temperature, respectively [26, 27],while the power factor (PF) is the product of square Seebeck coefficient and electrical conductivity ($S^2\sigma$). Hence, a large PF means that a device can output large voltage and large electrical current. When $ZT \geq 1$, the materials have a high potential of electric thermal performance.

In recent years, chimney ladder compounds (INCLs) have attracted increasing interest as promising thermoelectric (TE) materials because the compounds simultaneously realize a high power factor and a low thermal conductivity, as observed in higher manganese silicides (HMSs) [28, 29]. Moreover, the chemical bonding in T-E intermetallic provides a background for unusual physical properties, especially in the electronic transport, giving rise to narrow-gap semiconductors [30–35], high- and low-temperature thermoelectric materials [36–40], as well as superconductors [31–43]. This renders the T-E intermetallics promising functional materials for transport and thermoelectric applications.

S.V. Meschel [44] and his co-worker have measured the standard enthalpies of formation for some 5d transition metal silicides by high temperature direct synthesis calorimetry of $OsAl_2$. Moreover, Jiangling Pan et al. [45] have studied the doping of the transition metal Cr in the OsAl2 compounds to obtain magnetic alloys using first principles calculations. In another work [46], they investigated the electronic and magnetic properties of the transition metal aluminides XAl_2 in the $MoSi_2$ type structure by first-principle calculations. Recently, the structural and electronic properties of $RuAl_2$, $RuGa_2$, and $OsAl_2$ have been computed using the full potential linearized augmented plane wave (FP-LAPW) method by S. Laksari [47] and co-workers. After our careful research in the literature, there is no experimental work or theoretical research available of the thermoelectric properties concerning $OsAl_2$ compound, which represents the focus of this paper.

In the present work, the electronic and the thermoelectric properties of $OsAl_2$ were calculated using the full potential linearized augmented plane wave (FP-LAPW) method [48] based on density functional theory (DFT) [49–51]. Our results demonstrate that the thermoelectric properties are linked to their electronic structure. The different thermoelectric coefficients were then calculated for the first time, using computational code BoltzTrap [52].

2 Computational Details

The full potential linearized augmented plane wave plus local orbitals (FP-LAPW + lo) method was used and implemented in the Wien2K code [53] within the density functional theory [54]. The generalized gradient approximation GGA (PBE) [55] was employed for processing exchange correlation potential. Kohn–Sham equations based on FP-LAPW method have been solved. The energy cutoff − 6 Ryd is used for separating core states from valence ones. The cutoff energy for plane wave expansion (i.e., of wave functions in the interstitial region) is taken as $R_{MT}K_{MAX} = 8$, and number of k-points = 1000 has been considered. The wave functions inside atomic spheres are expanded with spherical harmonic up to $l_{max} = 10$.The radii of muffin-tin spheres were equal to 2.5 a.u. and 2.3 a.u. for Os and Al, respectively. The self-consistent is considered to be converged if the system energy is stable within 10^{-4} Ry. Thermoelectric properties have been calculated through the output files of WIEN2K code and by computational code BoltzTrap [52]. For the calculation of the transport properties, the thermoelectric self-consistent iterations were converged using a dense mesh of 40,000 k-points inside integral Brillouin cone (IBZ). A merit factor (ZT) is defined as $S^2\sigma$ T/K.

3 Results and Discussion

3.1 Structural and Electronic Properties

The existence of OsAl, $OsAl_2$, and Os_2Al_3 phases has been proven experimentally by X-ray analysis under the effect of a temperature higher than 1300 °C. Earlier, Esslinger and Schubert showed that OsAl adopted the CsCl-type structure, whereas the crystal structures of two other compounds $OsAl_2$ and Os_2Al_3 have been determined from single crystal X-ray characterization which confirmed that they have tetragonal structure type-$MoSi_2$, close to the CsCl-type structure. On the other hand, the structures type-$MoSi_2$ (C11), type-$CrSi_2$ (C40), and type-$TiSi_2$ (C54) are closely linked and can be described by an orthorhombic super-cell, which is composed of stacked planes in such a way to contain linear units MX_2. In the C11 and C54 structures, all the planes are parallel, while for the C40, each plane is in rotation relatively to the others. The stacking of atoms is repeated after two, three, and four respective planes, along the stacking direction, so that each M-type atom is surrounded by ten (10) X-type atoms, while the X-type atoms have a close neighbor arrangement consisting of five (5) X-type atoms and five (5) M-type atoms. Figure 1 shows tetragonal structure type-$MoSi_2$ with the space group I4/mmm [56] whose conventional mesh containing six (6) atoms is the most suitable configuration for the $OsAl_2$ compound.

The determination of equilibrium structures is the first and most fundamental step in all our calculations. High care is given to this as it will highly impact the quality of subsequent analyses. This compound has been studied in three different structural phases C_{11}, C_{40} and C_{54} and as shown in Fig. 2. We noted that the phase type-$TiSi_2$ is the most suitable. The analysis of the equilibrium structures are studied in our Ref. [47] where we found that the structure type-$TiSi_2$ more suitable for three compounds $OsAl_2$, $RuAl_2$, and $RuGa_2$ as shown in Fig. 2. But, in this topic, we are interested to analyze the different theoretical parameters just for $OsAl_2$ compound in the $MoSi_2$ type structure, because it is the most stable phase experimentally as cited in the Ref. [57]. The calculation has been achieved with GGA approximation. The equilibrium lattice parameters a and c, the bulk modulus B and its first derivative B', as well as other theoretical and experimental values are illustrated and compared in Table 1. Using the GGA approximation, the values of the lattice constants a and c are overestimated surrounding 0.50% and 0.82% for a and c, respectively, as compared to those found experimentally [57] and in good agreement with other theoretical work [56]. For the bulk modulus B, we did not succeed to found any experimental nor theoretical results for comparison purpose.

The investigation of electronic properties of the material will permit us to analyze and understand the nature of the

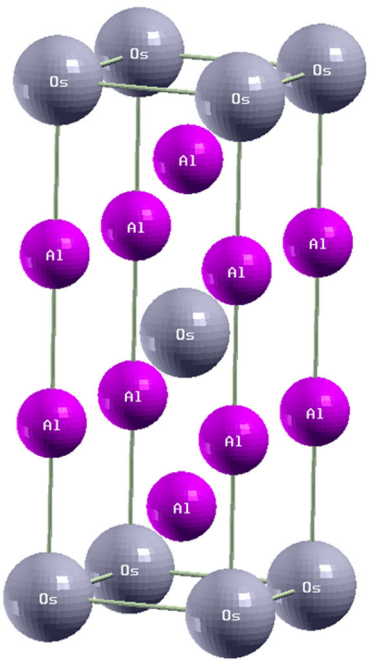

Fig. 1 Tetragonal structure type-$MoSi_2$ for $OsAl_2$ compound

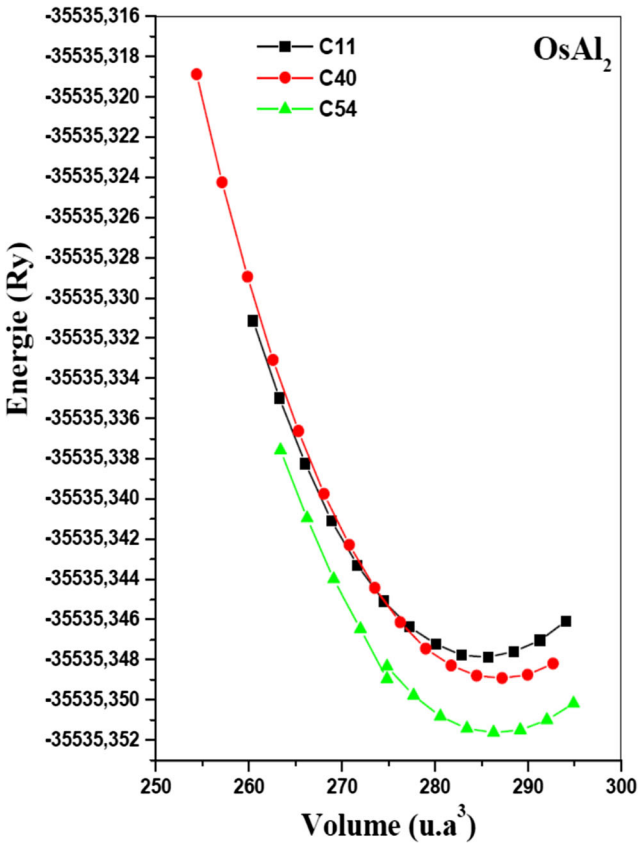

Fig. 2 The variation of energy as function of volume obtained with GGA in type-$MoSi_2$ (C11), type-$CrSi_2$ (C40) and type-$TiSi_2$ (C54) phases

Table 1 Lattice parameters a and c, bulk modulus B, and its derivate B' for $OsAl_2$ compound

	a (a.u)	c (a.u)	B_0 (GPa)	B′
Our cal	6.00	15.81	194.8128	4.62082
Exp	5.97[a]	15.68[a]	–	–
Other calculations	6.07[b], 6.37[c]	15.45[b]	–	–

[a] Ref. [57]
[b] Ref. [58]
[c] Ref. [45]

bonds that form between the different elements. These properties include the band structure and the density of state. We have calculated the energy band of our $OsAl_2$ compound along the high symmetrical direction in the Brillouin zone, and the results are presented in Fig. 3.

Figure 4 shows the calculated band gap of $OsAl_2$ with $MoSi_2$-type structure. The maximum of the valence band is found to be located in the ΓX direction, while the minimum of the conduction band is located in the UZ direction. Also, the indirect energy gap is calculated equal to 0.358 eV. These results demonstrate that the $OsAl_2$ compound has a semiconductor behavior, where the band gap is generated from the hybridization of Al p states with Os d states.

There are twenty-three (23) valence bands below the Fermi level and ten (10) conduction bands above it. The total and partial densities of states which are relative to the band structure are shown in Fig. 5. The low energy range [− 14 eV, − 5 eV] is mainly composed of *3s* and *3p* state electrons of Al, while the curve of the state density around Fermi level (from − 4 eV to Fermi surface) was mainly composed of *3d* state electron of Os and *3p* state electron of Al. The *3d* and *3p* states of Os and Al are located above the Fermi level, with a very weak contribution of *3s* in the total density. Therefore, the electrical transport property and the charge carrier type of $OsAl_2$ compound are governed mainly by *3d* and *3p* electrons.

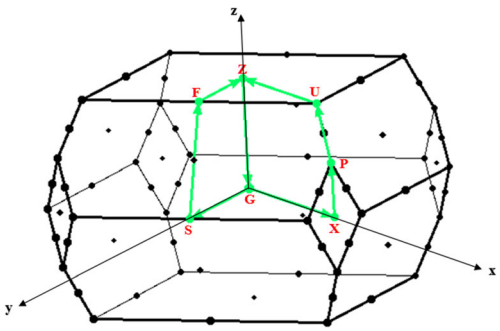

Fig. 3 High symmetrical direction in the first Brillouin zone

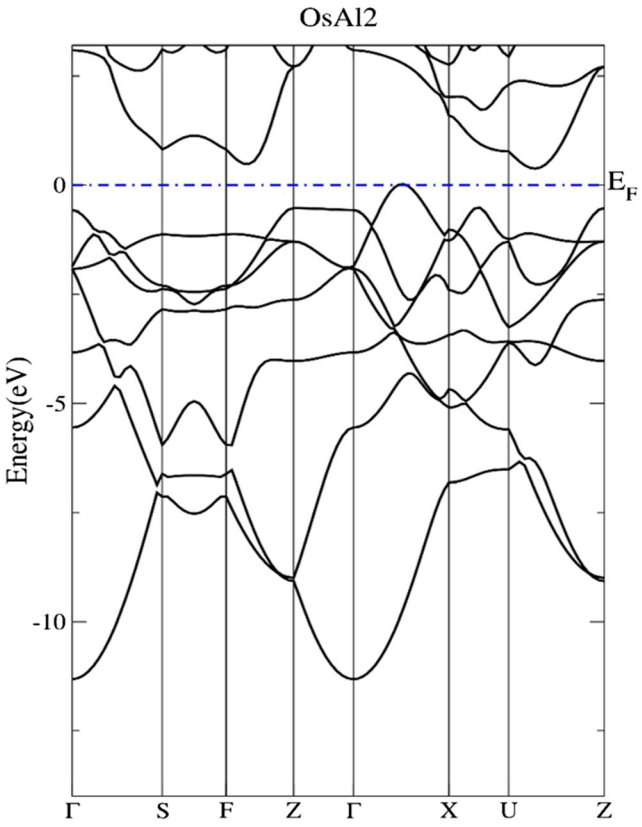

Fig. 4 Electronic band structure of $OsAl_2$ compound in tetragonal structure type-$MoSi_2$

3.2 Thermoelectric Properties

The different thermoelectrical coefficients were calculated as function of chemical potential (u) in the range from − 4 to 4 eV

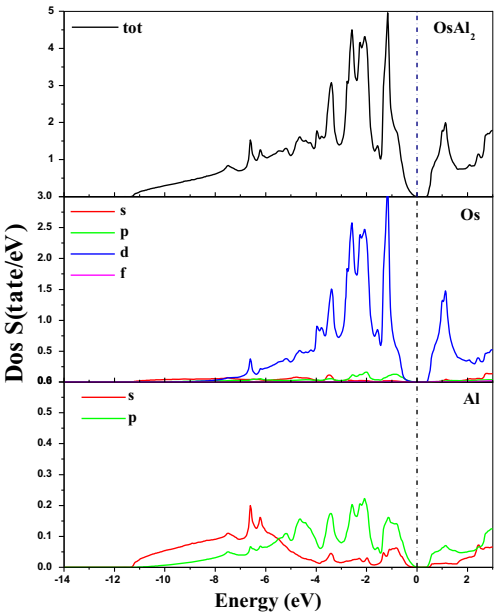

Fig. 5 Total and partial density of states for Os and Al in $OsAl_2$ compound

for the three considered temperatures, namely, 300, 600, and 900°K. The Seebeck coefficient S is an important factor to specify the type of semiconductor (n- or p-type), and it depends on the charge carrier concentrations (electrons versus holes).

Figure 6 shows the variation of S as a function of μ at temperatures of 300, 600, and 900 K for our $OsAl_2$ compound. We noted that the value of 539.5988 μV/K (− 592.4304 μV/K) for p- and n-type presented the maximum of S obtained at 300°K. The peak values decrease as the temperature increased due to the increase of electron and holes as a consequence of the thermal energy. These values are 292.6213 μV/K (− 366.2867 μV/K) and 285.084 μV/K (− 228.839 μV/K) for 600 k and 900 K in p- and n-region, respectively. The S values with n-type are higher than those calculated for p-type. Negative Seebeck values indicate that electron-type carriers dominate the thermoelectric transport. Finally, we suggest that the n-type compound title is more favorable for thermoelectric application than p-type.

Electrical conductivity σ allows electrical charges to pass freely through a solid or liquid body, in opposition to the electrical resistivity which slows the current. A high thermoelectrical performance requires a high value of electrical conductivity σ. The variations of electrical conductivity as a function of chemical potential μ for the range of temperature under study are presented in Fig. 7. We noticed that the shapes of the curves are somehow similar. The electrical conductivity has been found to be almost not affected by the temperature where the same behavior was observed (i.e., at 300, 600, and 900 K), while it was impacted by increasing the chemical potential. In the [0.05 eV, − 0.3 eV] range of μ, the σ value is equal zero for $T = 300$°K. In the considered chemical potential range, there is an important effect of electrical conductivity in the n-region for positive chemical potential than in the p-region for negative one. The maximum values of σ are 13.3×10^{20} and $5.714 \times 10^{20}\ \Omega^{-1}\ m^{-1}$ at 4 eV and − 2.13 eV in n-type and p-type regions, respectively.

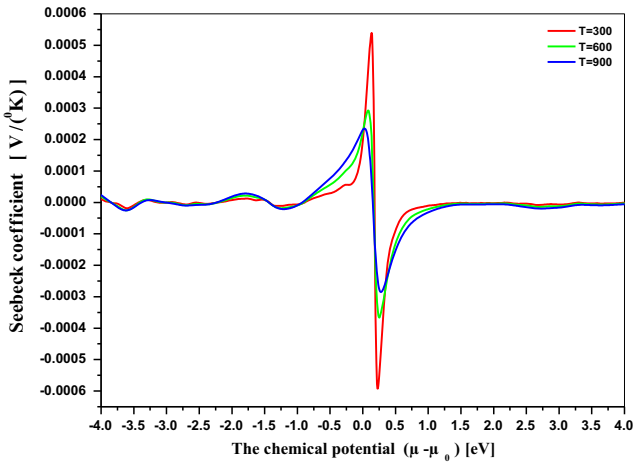

Fig. 6 Seebeck coefficient as a function of chemical potential at different temperatures of $OsAl_2$

The power factor PF depends on 2 key parameters, namely, the Seebeck coefficient and the electrical conductivity. These two quantities vary in opposite ways. This thermoelectric coefficient is defined by the following relation: $P = S^2\sigma$.The power factor relative to relaxation time as a function of chemical potential μ is presented in Fig. 8. The largest value occurred at 900°K and decreased with decreasing temperature. We notice two apparent peaks around the Fermi level, located at − 0.37 and 0.50 eV. The maximum thermoelectric PF is calculated at $12.38 \times 10^{11}\ W\ K^{-2}\ m^{-1}\ s^{-1}$ and is located at the 0.5 eV, while PF values of 7.772×10^{11} and $2.940 \times 10^{11}\ W\ K^{-2}\ m^{-1}\ s^{-1}$ are calculated at 600 and 300°K, respectively. The $OsAl_2$ compound has higher PF value in the n-type than in the p-type.

Similar to the electrical conductivity, the thermal conductivity indicates the capability of a material to let heat (analog to electron) flowing through it. Thermal conductivity κ is a constant. It is an intrinsic characteristic and is specific to each material. This coefficient can vary depending on the temperature and the humidity. Generally, the electrically insulating materials have κ between 0.025 and 0.050 W/m K. The TE materials are characterized by their low thermal conductivity κ.

The variation of κ as a function of chemical potential is plotted for temperatures of 300, 600, and 900°K, and the results are illustrated in Fig. 9. With increasing temperatures, κ increased, which is due to an increase of the free electrons energy and consequently the vibrational energy. The TE materials must have a large Seebeck coefficient S, high electrical conductivity σ, and low thermal conductivity κ [59]. At − 2.15 eV, and for p-type, the peak value located at 300°K is 4.134×10^{15} W/m K s, whereas the highest value located at 4 eV for n-type is 9.79×10^{15} W/m K s. At 900°K, the κ values in p-type and n-type are 11.233×10^{15} W/m K s (− 2.32 eV) and 294.32×10^{15} W/m K s (4 eV), respectively. With this comparison, we find out that the value corresponding to room temperature is more suitable for thermoelectric applications owing to the low thermal conductivity. Electrical and thermal conductivity are both sensitive to temperature. The thermal conductivity for $OsAl_2$ compound has a higher value in the n-type than in the p-type. The electrical conductivity has the same behavior because the maximum of both types coincide at the same chemical potential value which confirms that the Wiedemann-Franz law is verified [60].

In solid state, the electronic specific heat C_e (j/mol K) describes the contribution of electrons to the heat capacity. Heat is transported both by phonons and free electrons. According to the results displayed in Fig. 10 and showing the electronic specific heat as a function of chemical potential at different temperatures, the C_e increased with increasing temperature and reach its maximum value of 5.91 and 2.62 j/mol K at

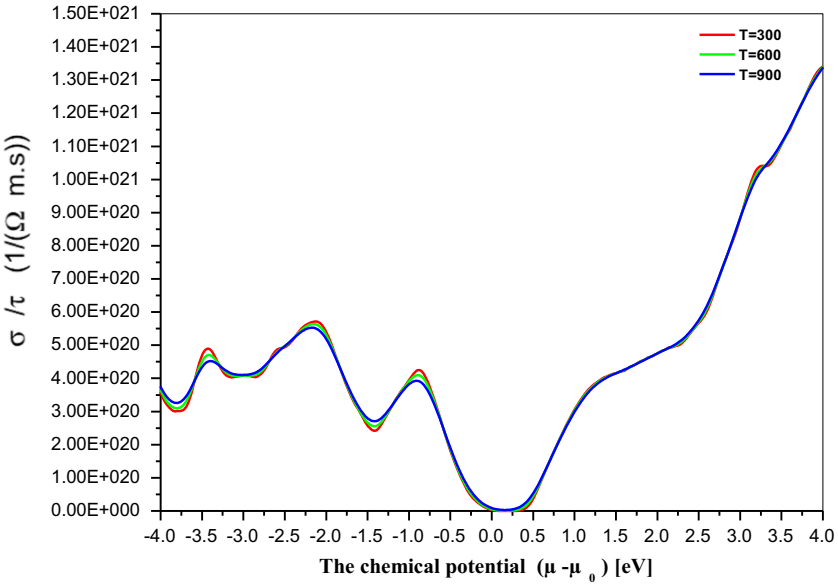

Fig. 7 Electrical conductivity as a function of chemical potential at different temperatures of $OsAl_2$

900°K, in negative and positive chemical potential, respectively. At room temperature, the maximum C_e is equal to 2.72 j/mol K and decreased to zero at 0.3 eV and then increases rapidly to 1.26 j/mol K.

The prediction of $OsAl_2$ compound for thermoelectric performance can be predicted by means of the figure of merit ZT. The ZT factor depends on Seebeck coefficient, electrical conductivity, and thermal conductivity. Figure 11 presents the variation of ZT as a function of the chemical potential calculated at 300, 600, and 900 K. We noted the same shape and similar behavior of ZT at all temperatures. However, the maximum value of ZT is about 0.90 and occurred at 0.27 eV for room temperature. These values decreased then slightly with increasing temperatures. This calculated high ZT value suggests strongly that our $OsAl_2$ compound has descent thermoelectric performance.

4 Summary

In summary, the structural and electronic properties of $OsAl_2$ semiconducting compound were investigated by density functional method. Our calculations were carried out using the PBE-GGA approximation. The obtained

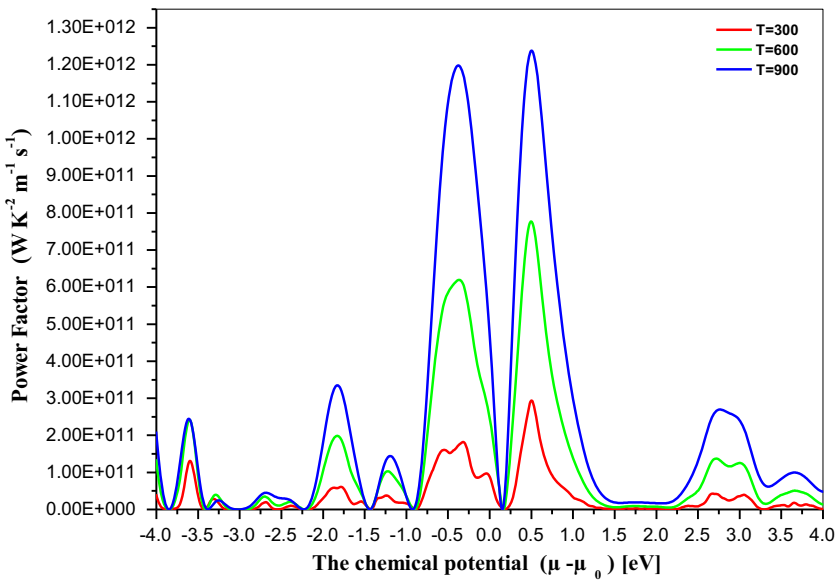

Fig. 8 Power factor as a function of chemical potential at different temperatures of $OsAl_2$

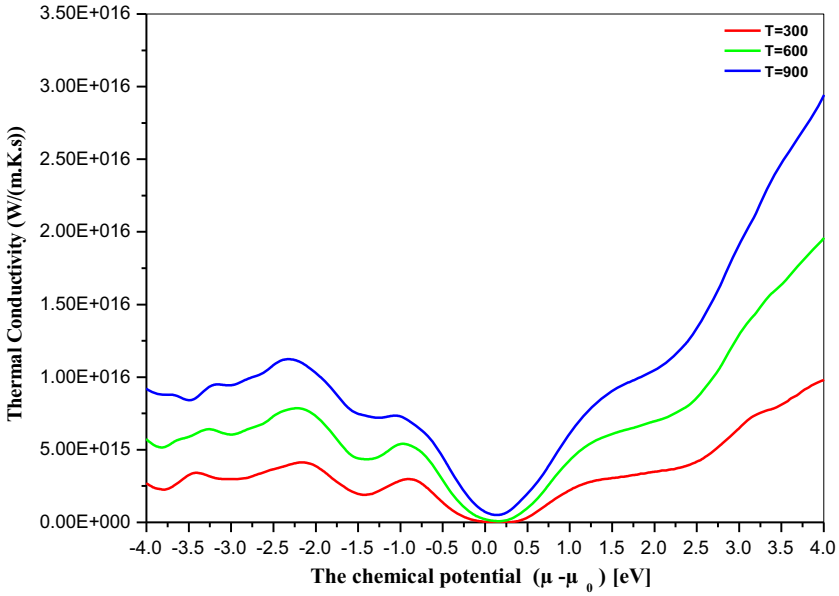

Fig. 9 Thermal conductivity as a function of the chemical potential at different temperatures of $OsAl_2$

results for lattice parameters *a* and *c* are in good agreement with previous relevant theoretical and experimental works. No experimental results were available in the literature data to allow us verifying our calculated indirect gap value (i.e., $E_g = 0.358$ eV) which corresponded to the structural phase C_{11} (tetragonal type-$MoSi_2$). To our best knowledge, the transport properties were calculated for the first time using Boltzmann transport theory. The different thermoelectric coefficients were studied at temperatures of 300, 600, and 900°K, where the high value of Seebeck coefficient was calculated at 300°K and suggested that the n-type compound like-type was more favorable than p-type. The electrical conductivity and thermal conductivity were found to increase with the increasing chemical potential. The $OsAl_2$ compound has high power factor PF in the n-region, and its ZT factor corresponded to 12.38×10^{11} W K^{-2} m^{-1} s^{-1} and 0.9, respectively. Our findings demonstrate that the $OsAl_2$ compound could be considered a very promising candidate for thermoelectric applications given its high thermoelectric performance.

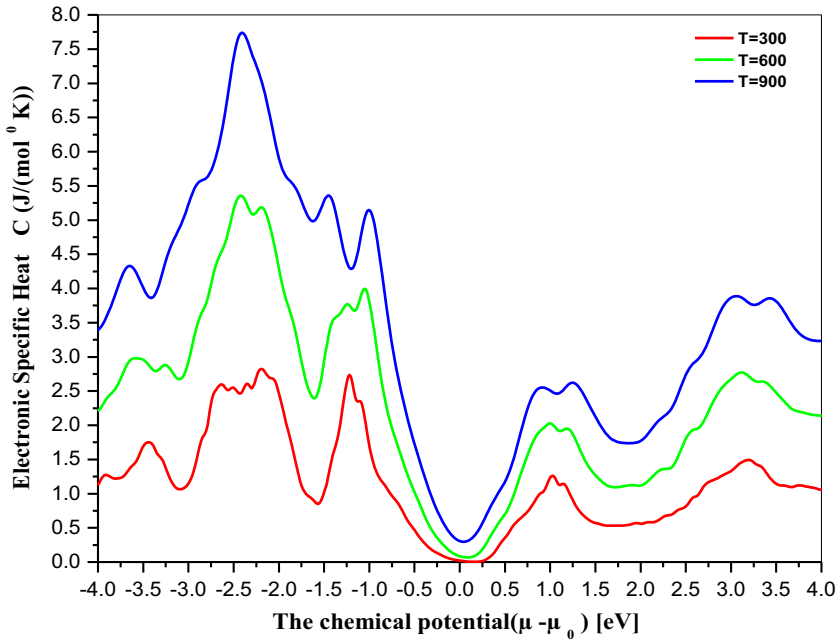

Fig. 10 The electronic specific heat as a function of the chemical potential at different temperatures of $OsAl_2$

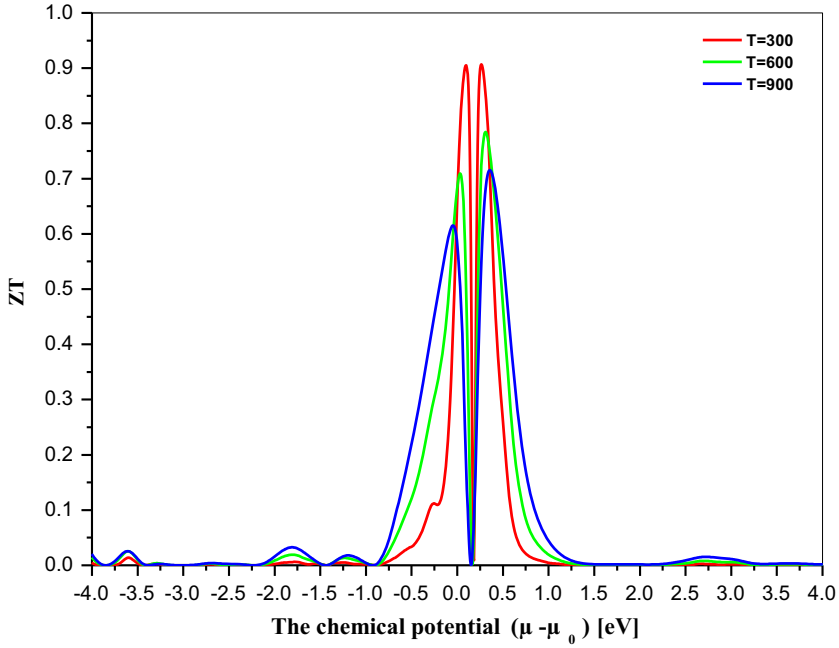

Fig. 11 Figure of merit ZT as a function of chemical potential at different temperatures of $OsAl_2$

Funding This work is supported by the Algerian University research project (PRFU) under grant number B00L02UN200120200001 and the General Directorate for Scientific Research and Technological Development (DGRSDT), Algeria.

References

1. Sekkal, A.: Etude ab initio des propriétés physiques et les effets de défaut dans les composés intermétalliques a base de terre rare, Thèse de Doctorat de l'Université de Tlemcen, (2014)
2. Chouhan, S.S., Soni, P., Pagare, G., Sanyal, S.P., Rajagopalan, M.: Physica B. **406**, 339 (2011)
3. Stoloff, N.S., Liu, C.T., Deevi, S.C.: Intermetallics. **8**, 1313 (2000)
4. Berdovsky, Y.N.: Intermetallics research progress, p. 1. Nova science publishers, Inc., New York (2008)
5. T.J. Seebeck; Abhandlungen der Deutschen Akademie der Wissenschafren zu Berlin 265 (1821) 1822
6. J.C. Peltier: Ann. Chim. LVl (1834) 371
7. Thomson, W.: Proceedings of the Royal Society of Edinburgh, p. 91. Royal Society of Edinburgh, Edinburgh (1851)
8. Candolfi C.: Synthèse, caractérisation physico-chimique et propriétés de transport de composés de type Mo3Sb7. Thèse de Doctorat de l' de l'Institut National Polytechnique de Lorraine (2008)
9. H. Nowotny, in: The chemistry of extended defects in non metallic solids, edited by E.R.Eyring, M.O'Keefe (North - Holland, Amsterdam) (1970) 223
10. Pearson, W.B.: Acta Cryst. B. **26**, 1044 (1970)
11. Fredrickson, D.C., Lee, S., Hoffmann, R., Lin, J.: Inorg. Chem. **43**, 6151 (2004)
12. Fredrickson, D.C., Lee, S., Hoffmann, R.: Inorg. Chem. **43**, 6159 (2004)
13. Vining, C.B.: AIP Conf. Proc. **246**, 338 (1992)
14. Arita, Y., Mitsuda, S., Nishi, Y., Matsui, T., Nagasaki, T.: J. Nucl. Mater. **294**, 202 (2001)
15. Ivanenko, L., Filonov, A., Shaposhnikov, V., Behr, G., Souptel, D., Schumann, J., Vinzelberg, H., Plotnikov, A., Borisenko, V.: Microelectronic Eng. **70**, 209 (2003)
16. Simkin, B.A., Hayashi, Y., Inui, H.: Intermetallics. **13**, 1225 (2005)
17. Simkin, B.A., Ishida, A., Okamoto, N.L., Kishida, K., Tanaka, K., Inui, H.: Acta Mater. **54**, 2857 (2006)
18. Imai, Y., Watanabe, A.: Intermetallics. **13**, 33 (2005)
19. C. P. Susz, J. Muller, K. Yvon and E. Parthé: J. Less – Common Met. 71 (1980) 1
20. Gottlieb, U., Sulpice, A., Lambert-Andron, B., Laborde, O.: J. Alloys Compd. **361**, 13 (2003)
21. Schwomma, O., Preisinger, A., Nowotny, H., Wittman, A.: Monatsch Chem. **95**, 527 (1964)
22. Knott, H.W., Mueller, M.H.: Heaton I. Acta Crystallogr. **23**, 549 (1967)
23. Ivanenko, L., Filonov, A., Shaposhnikov, B., Behr, G., Souptel, D., Schumann, J., et al.: Microelectron. Eng. **70**, 209 (2003)
24. Souptel, D., Behr, G., Ivanenko, L., Vinzelberg, H., Shumann, J.: J. Cryst. Growth. **244**, 296 (2002)
25. Zaitsev, V.K.: Thermoelectric properties of anisotropic MnSi1.75. In: Rowe, D.M. (ed.) CRC handbook on thermoelectrics, p. 299. CRC Press, New York (NY) (1994)
26. Fedorov, M.I., Zaitsev, V.K.: Thermoelectrics of transition metal silicides. In: Rowe, D.M. (ed.) Thermoelectrics handbook, pp. 31–33. CRC Press, Boca Raton (2006)
27. Miyazaki, Y., Kikuchi, Y.: Higher manganese silicide, MnSig. In: Koumoto, K., Mori, T. (eds.) Thermoelectric nanomaterials. Springer Series in Materials Science, pp. 141–156. Springer, Berlin (2013)
28. Zhou, A.J., Zhu, T.J., Zhao, X.B., Yang, S.H., Dasgupta, T., Stiewe, C., Hassdorf, R., Mueller, E.: J. Electron. Mater. **39**, 2002 (2010)
29. Kikuchi, Y., Miyazaki, Y., Saito, Y., Hayashi, K., Yubuta, K., Kajitani, T.: Jpn. J. Appl. Phys. **51**, 085801 (2012)
30. Häussermann, U., Boström, M., Viklund, P., Rapp, Ö., Björnängen, T.: FeGa3 and RuGa3: semiconducting intermetallic compounds. J. Solid State Chem. **165**, 94 (2002)

31. Bogdanov, D., Winzer, K., Nekrasov, I.A., Pruschke, T.: Electronic properties of the semiconductor RuIn3. J. Phys.: Condens. Matter. **19**, 232202 (2007)
32. Evers, J., Dehlinger, G., Meyer, H.: Semiconducting behavior of RuGa2. Mat. Res. Bull. **19**, 1177 (1984)
33. Paschen, S., Felder, E., Chernikov, M.A., Degiorgi, L., Schwer, H., Ott, H.R., Young, D.P., Sarrao, J.L.: Fisk, Z. Phys. Rev. B. **56**, 12916 (1997)
34. Petrovic, C., Kim, J.W., Bud'ko, S.L., Goldman, A.I., Canfield, P.C., Choe, W., Miller, G.J.: Phys. Rev. B. **67**, 155205 (2003)
35. Sales, B.C., May, A.F., McGuire, M.A., Stone, M.B., Singh, D.J.: Mandrus, D. Phys. Rev. B. **86**, 235136 (2012)
36. Wagner, M., Cardoso-Gil, R., Oeschler, N., Rosner, H., Grin, Y.: J. Mater. Res. **26**, 1886 (2011)
37. Kasinathan, D., Wagner, M., Koepernik, K., Cardoso-Gil, R., Grin, Y., Rosner, H.: Phys. Rev. B. **85**, 035207 (2012)
38. Wagner-Reetz, M., Kasinathan, D., Schnelle, W., Cardoso-Gil, R., Rosner, H., Grin, Y.: Phys. Rev. B. **90**, 195206 (2014)
39. Tomczak, J.M.; Haule, K.; Kotliar, G. NAPSB. (2013) 45
40. Sun, P., Oeschler, N., Johnsen, S., Iversen, B.B., Steglich, F.: Dalton Trans. **39**, 1012 (2010)
41. Shibayama, T., Nohara, M., Katori, H.A., Okamoto, Y., Hiroi, Z., Takagi, H.: J. Phys. Soc. Jpn. **76**, 073708 (2007)
42. Xie, W., Luo, H., Phelan, B.F., Klimczuk, T., Cevallos, F.A., Cava, R.J.: PNAS. **112**, 7048 (2015)
43. Verchenko, V.Y., Tsirlin, A.A., Zubtsovskiy, A.O., Shevelkov, A.V.: Phys. Rev. B. **93**, 064501 (2016)
44. Meschel, S.V., Kleppa, O.J.: J. Alloys Compd. **280**, 231 (1998)
45. Pan, J., Ni, J., Yang, B., Dai, Z.: Phys. Lett. A. **374**, 4909 (2010)
46. Pan, J., Ni, J., Yang, B.: Comput. Mater. Sci. **50**, 2433 (2011)
47. Laksari, S., Khatir, R., Rozale, H., Mebsout, R., Mokadem, A., Sayede, A., Chahed, A., Benhelal, O.: Comput. Mater. Sci. **61**, 20 (2012)
48. Singh, D.J.: Plane waves, pseudopotentials and the LAPW method. Kluwer Academic, Boston (1994)
49. Hohenberg, P., Khon, W.: Phys. Rev. **136**, B864 (1964)
50. Khon, W., Sham, L.J.: Phys. Rev. **140**, A1133 (1965)
51. Sham, L.J., Khon, W.: Phys. Rev. **145**, 561 (1965)
52. Madsen, G.K.H., Singh, D.J.: Comput. Phys.Commun. **175**, 67 (2006)
53. Blaha, P., Schwarz, K., Madsen, G.K.H., Kvasnicka, D., Luitz, J.: WIEN2K, an augmented plane wave plus local orbitals program for calculating crystal properties. Vienna University of Technology, Vienna (2001)
54. Hohenberg P, Kohn W. Phys Rev B 1964; 136:864. W. Kohn, L. J. Sham, Phys. Rev. B 140 (1965) 1133
55. Monkhorst, H.J., Pack, J.D.: Phys. Rev. B. **13**, 5188 (1976)
56. Hill, R.J., Craig, G.R., Gibbs, G.V.: Phys. Chem. Minerals. **4**, 317 (1979)
57. Lars-Erik Edshammar - Acta Chemica Scandinavica.19 (1965) 871
58. Springborgy, M., Fischerz, R.: J. Phys.: Condens. Matter. **10**, 701 (1998) Printed in the UK
59. Snyder, G.J., Toberer, E.S.: Complex thermoelectric materials. Nat. Mater. **7**, 105 (2008)
60. Zhang, J., et al., Phosphorene nanoribbon as a promising candidate for thermoelectric applications 2014. arXiv preprint arXiv: 1405.3348